JOURNAL OF PROPULSION AND POWER
Vol. 21, No. 5, September–October 2005

Nacelle Interaction with Natural Wind Before Takeoff

C. A. Hall* and T. P. Hynes†
University of Cambridge, Cambridge, England CB2 1PZ, United Kingdom

To understand how natural wind close to the ground interacts with a jet engine, tests have been completed with a 1/20-scale model fan and intake rig operating within a simulation of the lower atmospheric boundary layer. Unsteady measurements are used to confirm that turbulence in the ambient flow is attenuated as the intake is approached, and analysis of unsteady pressure data reveals that the nacelle surface pressure field is most sensitive to large length-scale gusts. A new statistical approach to analyze intermittent intake separation is used to show that there is hysteresis in the unsteady separation and reattachment of the inlet flow and that there are similarities between the unsteady and steady intake performance. These findings suggest that the intake response to natural wind can be described as quasi steady, and a novel probabilistic model of nacelle behavior is devised based on this hypothesis. The model shows that by combining some statistical characteristics of the wind with the steady intake performance it is possible to synthesize the observed unsteady performance. This confirms that the intake response can be treated in a quasi-steady manner, and this has significant practical implications for engine intake testing and design.

Nomenclature

C_p	=	surface pressure coefficient
D_1	=	intake highlight diameter
G_r, G_s	=	gusts of wind initiating reattachment and separation of the inlet flow, respectively
H	=	reference height for wind data; 10 m at full scale
h	=	height of the rig or engine centerline
I_i	=	turbulence intensity component, $\sigma_i U$, where $i = u$, v, or w
$i(t)$	=	fluctuating component of velocity
L_i	=	integral length scale of turbulence
L_q	=	size of the captured stream tube in the far field
$\dot{m}$	=	mass flow rate through the rig/engine
n	=	frequency
$P(X)$	=	probability of event X occurring
p, p_0	=	static pressure, stagnation pressure
$p(i)$	=	probability density function of parameter i
Q	=	binary variable defining state of intake flowfield, with attached flow, 0; with separated flow, 1
Re	=	Reynolds number for the intake flow
$S_{ii}(n)$	=	power spectral density function of component i
T	=	averaging time
t	=	time
U	=	time-averaged streamwise velocity
$u(t)$	=	fluctuating streamwise velocity component
V_∞	=	far-field characteristic wind speed
$v(t)$	=	lateral velocity component
$w(t)$	=	normal velocity component
z	=	vertical coordinate from ground plane
z_0	=	surface roughness height, m
α	=	wind direction relative to the rig centerline
Δt	=	quasi-steady gust duration
ρ	=	density
σ_i	=	standard deviation of parameter i
ϕ	=	fan flow coefficient

Subscripts

att	=	value with attached inlet flow
i	=	fluctuating velocity component u, v, or w
PS	=	value at the peak suction point on the inlet lip
r, s	=	value for inlet flow reattachment, separation
sep	=	value with separated inlet flow
∞	=	far-field value in the natural wind

Presented as Paper 2002-3773 at the AIAA/ASME/SAE/ASEE 38th Joint Propulsion Conference and Exhibit, Indianapolis, IN, 7 July 2002; received 21 May 2004; revision received 24 February 2005; accepted for publication 24 February 2005.

*Research Associate, Department of Engineering, Trumpington Street. Member AIAA.

†Senior Lecturer, Department of Engineering, Trumpington Street.

I. Introduction

THE atmospheric flow encountered by the engines of a passenger aircraft during the preparation for takeoff can be highly unsteady and gusting. This unsteadiness is potentially troublesome for engine operation, but it is neglected in the steady tests and computations that are typically used to examine engine performance in crosswind. There is a need to improve our understanding of the behavior of jet engines operating within real-world situations, and this is the overall purpose of this research.

There are two specific questions that this paper sets out to answer: First, how does turbulent, atmospheric flow distort as it approaches the intake of a jet engine? Second, can the performance of an intake operating in unsteady flow be related to its steady characteristics that are more easily determined and understood?

To answer these two questions, a novel experiment is presented, in which a model rig representing an engine fan and intake was operated within a simulation of atmospheric flow close to the ground. Unsteady velocity measurements are used to follow the modification of the turbulence, and statistical analysis of intermittent flow separation is applied to characterize the intake unsteady performance. The test conditions used for this experiment were carefully controlled so that they were equivalent to the operating conditions used for previous steady flow tests. This enables the effects of atmospheric turbulence on the intake performance to be isolated.

In terms of previously published work, there is very little in the field of engine operation within unsteady flow conditions. Freeman and Rowe[1] demonstrated the complex behavior of a large turbofan engine operating in atmospheric flow. They presented engine test measurements that showed the intake flow separating intermittently in natural wind. In some instances, a dynamic interaction was observed between the wind, the intake flow, and the fan and installation that could lead to fan stall events.

There are, however, many studies available of the interaction of turbulent flowfields with structures. Many of these suggest that the critical characteristic of the turbulence is the integral length scale L_u. If this is larger than the size of the object, then the flow can usually be treated as quasi-steady, and the variation in desired quantities

should then correlate with the turbulence intensity σ_u, for example, as described in Ref. 2. This same reasoning cannot, however, be applied to our problem, despite the fact that, for an engine intake in wind, the turbulence length scale is much larger than the size of the engine. The principal difference is that the engine does not respond passively to the oncoming turbulence. The strong contraction in the flow entering the intake distorts the turbulence field. If nonlinear and viscous effects are neglected, this distortion of the turbulence can be analyzed with a method known as rapid distortion theory (RDT). Many examples of RDT being applied to the interaction of a turbulent stream with a structure can be found in the literature.[3,4] These studies show the application of RDT to be appropriate when the distortion of the mean flowfield is high and the scale of the turbulence is relatively small. The results obtained in this paper indicate that any fluctuations at scales smaller than about the size of the captured stream tube are effectively filtered out, as predicted by RDT, and it is the properties of the wind after this filtration to which the intake responds.

The structure of the paper is as follows: We will first present results to demonstrate that we have achieved an appropriate model-scale simulation of an atmospheric boundary layer. We will then investigate how this turbulent flow distorts as it approaches a model intake and show that the changes are broadly consistent with what one would expect from RDT considerations. Based on this and on measurements of the response of the flow around the intake lip, we will argue that the appropriate length scales on which to view the flow are of the order of the size of the captured stream tube. The characteristics of the measured intermittent separation are then examined, and the results show, similarly to the steady tests, the importance of hysteresis in the separation–reattachment cycle. They also indicate that the intake response can be described as quasi steady, and a model is proposed based on this hypothesis. The model shows that by combining some of the statistical characteristics of the unsteady wind with the known steady intake performance it is possible to reproduce the measured unsteady performance. This demonstrates that the intake behavior is indeed quasi steady.

This paper represents the first comprehensive study of the interaction between atmospheric turbulence close to the ground with an operating engine intake. It makes a contribution to the field of turbulence interaction with a non-passive structure and, more significantly, to the subject of engine operation within unsteady conditions. The findings have implications for improved engine test and operational procedures, and they could lead to future fan and intake designs that are better suited to the real conditions perceived by engines in commercial operation.

II. Experimental Method

The model fan and nacelle rig used for the experiments is described in Ref. 5. The environmental wind tunnel at the Osney Laboratory in Oxford was used for all of the experiments.[6] Upstream of the tunnel turntable, turbulence generators, in the form of house bricks, were arranged on the floor in a regular pattern. At the tunnel entrance, a large wooden grid was fitted, also to generate turbulence. To determine a suitable wind-tunnel configuration, several combinations of roughness elements and upstream grid were assessed.

The aim was to reproduce the characteristics given by the correlations of the Engineering and Science Data Unit (ESDU), for a surface roughness height of 0.03 m at the model rig scale of 1/20 (Ref. 7). This wind is typical of open country terrain, and it was deemed to be most representative of the atmospheric flow above an airport runway.[8] The description of the wind given by ESDU is known as the mean hourly wind. This is an equilibrium turbulent flow in which the statistics are stationary. A period of 1 h at full scale is chosen because changes in the weather typically take several hours to occur. In this context, the weather determines the mean wind speed and direction but does not influence the turbulence characteristics.

The final tunnel configuration used for all of the unsteady experiments is shown in Fig. 1. The rig scale and the range of tunnel speeds used produces a simulation in which the timescale of the

Fig. 1 Unsteady experiment setup within the Osney Laboratory environmental wind tunnel.

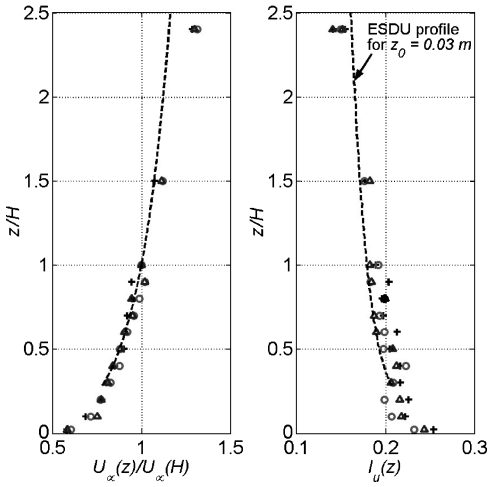

Fig. 2 Measured profiles of ABL simulation compared with ESDU correlations.

experiments was about one-sixth of a full-scale wind, and therefore, a tunnel experiment lasting 10 min corresponded to an engine test of 1 h.

The nondimensional parameters representing a simulation of the lower atmospheric boundary layer (ABL) can be listed as follows:

$$\mathrm{ABL} = f\left\{\frac{nS_{ii}(n,z)}{\sigma_i(z)^2}, \frac{L_i(z)}{D_1}, \frac{\sigma_i(z)}{V_\infty}, \frac{U(z)}{V_\infty}\right\} \tag{1}$$

that is, nondimensional turbulence power spectral density, integral length scale, strength of turbulence, and wind mean profile, respectively, and where the index i runs over the three fluctuating velocity components. To reproduce the flowfield exactly, all of these groups must be matched at the scale of the simulation, and the ability to reproduce these characteristics in the wind tunnel indicates the quality of the simulation. For a given value of surface roughness height, ESDU provides correlations for all of the statistical parameters in Eq. (1).

Figure 2 shows the measured mean velocity and the streamwise turbulence intensity profiles for the atmospheric simulation. The results are measured at three different tunnel speeds and compared with the correlations given in Ref. 7. The level of agreement demonstrated was judged to be good for an atmospheric simulation.

Note that $U_\infty(H)$ is the far-field mean flow velocity at the reference height H. This is the standard measure of the wind speed used within wind engineering. The characteristic wind speed V_∞ is the area-averaged value of $U_\infty(z)$ for the freestream air that enters the intake captured stream tube.

Figure 3 shows the measured streamwise spectra for the simulation as functions of reduced frequency. The measured distributions

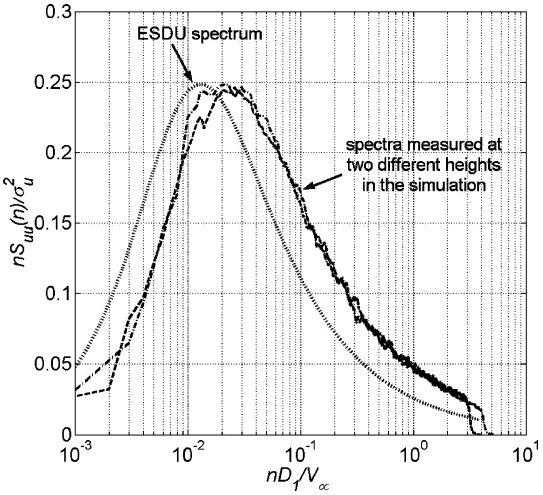

Fig. 3 Measured and correlated streamwise velocity spectra of atmospheric simulation as a function of nondimensional frequency.

collapse onto one curve that has a very similar shape to the target distribution. The horizontal shift of this from the target spectra shows the difference between the scale of the simulation and the scale of the model rig. The simulation is about one-half the size of that required, which is a consequence of the wind tunnel not being large enough to generate very long length scales. Of greatest importance to this work is whether there are fluctuations that vary in size from being smaller than the intake diameter, $nD_1/V_\infty > 1$, to much larger than the intake diameter, $nD_1/V_\infty \ll 1$. This is clearly the case, and therefore, the simulation was deemed more than adequate for this study.

Given that the characteristics of the simulated atmospheric flow are fixed, the statistics of any aerodynamic quantities that can be measured are functions of the following experimental variables:

$$P(\text{sep}) = f\{Re, (h/D_1), \bar{\alpha}, \phi, (\overline{L_q}/D_1)\} \tag{2}$$

where $P(\text{sep})$ represents the probability of the intake flow being separated.

These parameters are comparable with those for the rig in a steady, uniform crosswind; see Eq. (1) in Ref. 5. The stream-tube contraction ratio and the wind direction are the only experimental variables changed by the unsteadiness of the wind-tunnel flow, and to make these parameters equivalent, time-average quantities are used (denoted by overbars). The time averaging is applied such that any pair of steady and unsteady experiments with the same values of these parameters will also have the same mean flowfields. Note that for both steady and unsteady flow the captured stream-tube size is defined as $\overline{L_q} = \sqrt{(\dot{m}/\rho V_\infty)}$.

III. Distortion of the Unsteady Flowfield

Particle image velocimetry (PIV) and hot-wire measurements were used to investigate the characteristics of the flow upstream of the intake. The experiments were aimed at investigating how the complex, turbulent flow in the lower atmospheric boundary layer distorts as an engine intake is approached.

PIV images provide excellent flow visualisation, and Fig. 4 shows an instantaneous view of the turbulent field approaching the rig. This photograph effectively captures the smaller-scale flow features that lie within the plane of the laser sheet. The rapid contraction of the flow into the intake is immediately apparent: The highly straining flow appears to be squeezing the turbulence out of the flowfield as it enters the nacelle.

Such images are strong evidence of the small-scale turbulence undergoing rapid distortion within the mean flow-field of the intake. In other words, the rapid acceleration is stretching and reorienting the smaller-scale turbulence as it enters the engine. The eddies exposed by the photograph are smaller than the nacelle diameter, but as Fig. 3 indicates, there are also fluctuations present that are much larger than the engine. (The streamwise integral length scale close

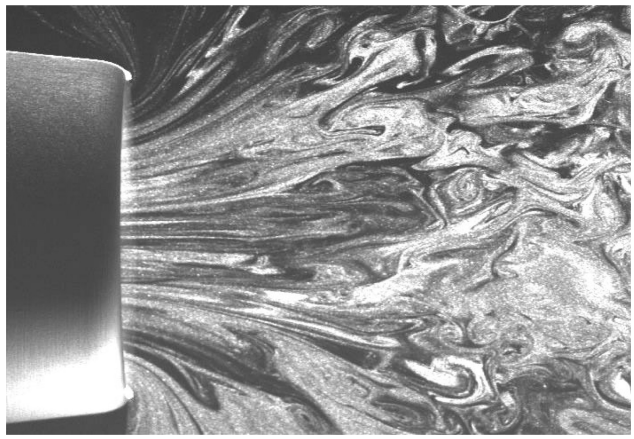

Fig. 4 PIV image of intake flow with axisymmetric mean flow, $\bar{\alpha} = 0^0$, $h/D_1 = 3$, $\overline{L_q}/D_1 = 4$.

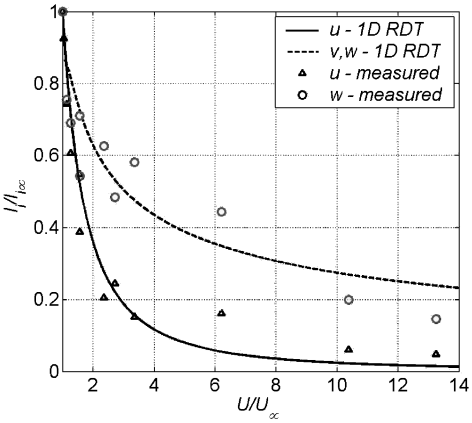

Fig. 5 Measured turbulence intensity levels approaching the model rig compared with simple RDT.

to the ground is about 50 m at full scale.) These are not resolved by the photograph, and the full spectra of turbulence was investigated using hot-wire measurements.

A two-axis cross wire was used to measure the fluctuating velocities in front of the rig. The hot wire was traversed along a mean streamline from a position in the far-field wind to the highlight plane of the inlet. There were 10 min of hot-wire data recorded at each location with the rig operating at the required operating condition.

In Fig. 5 measurements are presented from two experiments with different values of stream-tube contraction ratio, $\overline{L_q}/D_1$. The results of two traverses are shown in terms of how the turbulence intensity varies with the local flow speed. The RDT of Batchelor[9] provides a theoretical prediction for the modification of turbulence intensity components for flow passing through a one-dimensional contraction:

$$(I_u/I_{u\infty})^2 = (3/4c^4)\{[(1+\kappa^2)/2\kappa^3]\,\ell n[(1+\kappa)/(1-\kappa)] - 1/\kappa^2\} \tag{3}$$

$$(I_v/I_{v\infty})^2 = (I_w/I_{w\infty})^2 = 3/4c + (3/4c^4)\{1/2\kappa^2 - [(1-\kappa^2)/4\kappa^3]\,\ell n[(1+\kappa)/(1-\kappa)]\} \tag{4}$$

where $\kappa^2 = 1 - c^{-3}$ and $c = U/U_\infty$.

The results from these equations are also in Fig. 5. The measured results show good agreement with this model, suggesting that to a first approximation the turbulence distorts as though it is passing through a rapid one-dimensional contraction. The magnitude of this contraction varies in space, and it is determined by the mean flowfield. Figure 5 shows that the streamwise velocity fluctuations are reduced more than fluctuations normal to the streamwise direction. The streamwise turbulence intensity at the intake face is less than 10% of the value in the far field.

IV. The Response of the Intake Lip to Unsteadiness

The response of the nacelle to the local velocity field is an example of fluid–structure interaction in which the flow is unsteady and random and the structure is rigid. Such problems are conventionally tackled by examining the admittance functions relating the unsteadiness in the flow to the surface pressure fluctuations. In this study, the pressure response is complicated by the very three-dimensional nature of the flowfield close to the intake and by intermittent flow separation. Therefore, the pressure response is examined by first looking at the case when the crosswind angle is zero (as considered in the preceding section).

Figure 6 shows spectra for the pressure fluctuations measured at the top dead center of the nacelle highlight compared with the spectra of the velocity components measured at the same time close to the highlight. All of the spectra are smooth functions and free from electrical noise (apart from a spike caused by the drive motor). The velocity spectra can be compared with those measured in the far field (Fig. 3), and it is seen that the peak in the streamwise velocity spectrum has moved to a higher frequency. The pressure spectrum closely follows the streamwise velocity spectrum. This suggests that the surface pressure field responds directly to the local streamwise velocity fluctuations over a wide range of frequencies without any selective amplification.

Figure 7 shows aerodynamic admittance functions relating static pressure at the highlight to velocity fluctuations close to the intake lip and to velocity fluctuations measured in the far field. The top curve confirms the findings from Fig. 6 that the pressure field responds to the streamwise velocity fluctuations equally for the whole frequency range. The lower curve suggests that the lip pressure is most sensitive to streamwise fluctuations in the far field that are larger than the capture stream tube $nD_1/V_\infty \sim 0.3$ (or $nL_q/V_\infty \sim 1$). The peak in the response is caused by the upward shift in frequency of the streamwise velocity spectrum and by the rapid distortion of the higher frequencies.

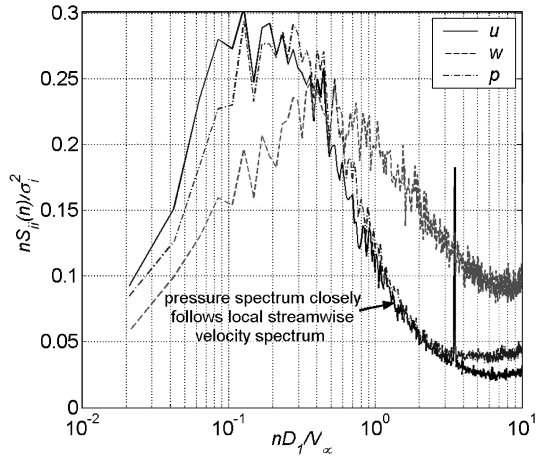

Fig. 6 Spectra of local velocity components compared to highlight pressure spectrum, $Re = 3 \times 10^5$, $h/D_1 = 1.25$, $\overline{L_q}/D_1 = 3$, and $\bar{\alpha} = 0$ deg.

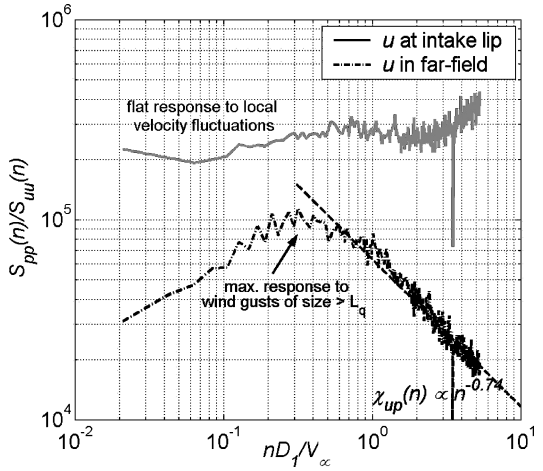

Fig. 7 Admittance functions relating lip pressure to streamwise velocity at highlight and far field, $Re = 3 \times 10^5$, $h/D_1 = 1.25$, $\overline{L_q}/D_1 = 3$, and $\bar{\alpha} = 0$ deg.

Figures 6 and 7 demonstrate that the overall effect of the mean acceleration of the flow is to attenuate and filter the turbulent fluctuations in the wind. The smaller eddies that can be contained within the capture stream tube are most strongly distorted, and this is demonstrated by the rate of falloff at high frequency of the lower admittance function in Fig. 7. The best-fit line through the data suggests the following relationship:

$$S_{pp}(n) \propto [S_{ii}(n)]_\infty n^{-0.7} \qquad \text{for} \qquad nD_1/V_\infty > 1 \tag{5}$$

Bearman[10] also measured an attenuation of the pressure spectra relative to the velocity fluctuations in front of a two-dimensional bluff body. This attenuation combined with the overall shift in the frequency spectrum confirms that larger-scale fluctuations are most significant to the intake pressure field.

V. Characteristics of Intermittent Inlet Separation in Unsteady Crosswind

Pressure measurements at 14 positions along the nacelle surface were recorded continuously with the rig operating in simulated natural wind conditions. The pressure tappings were located at the most windward part of the intake, and the channels were logged simultaneously at a frequency of 10-Hz for 10-min duration.

Figure 8 shows a sample of the resulting pressure distribution around the windward side of the nacelle for a mean crosswind angle of 30 deg. Measurements in unsteady flow at several time instances are shown, as well as the pressure distribution for the rig operating at the equivalent steady condition. Note that the steady distribution is contained within the envelope of unsteady pressure fluctuations and that the intake flow appears to be simply flipping between two distinct regimes: one corresponding to attached and one to separated flow. As long as the flow is attached, the nacelle surface pressure field is not radically altered by the unsteadiness in the flow. In both steady and unsteady cases, the flow accelerates around the highlight to the point of peak suction, which is just downstream. From this point, the flow diffuses continuously up to the fan face. When the flow is separated, the static pressure distribution is almost constant from the highlight to the throat, with some diffusion downstream as the fan face is approached. A similar distribution is seen in steady separated flow; see Fig. 3 in Ref. 5.

The intake surface pressure distribution can be characterized using a lip diffusion factor (DF_{ps}). This diffusion factor is defined using the peak suction pressure measurement,

$$DF_{ps} = (V_{ps} - V_{th})/V_{ps} \tag{6}$$

where $V = \sqrt{[2(p_{0\infty} - p)/\rho_\infty]}$.

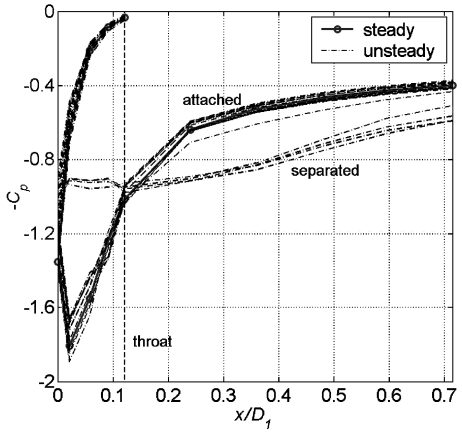

Fig. 8 Unsteady and steady surface pressure distributions at windward lip, $Re = 3 \times 10^5$, $h/D_1 = 1$, $\overline{L_q}/D_1 = 3$, $\phi = 0.62$, and $\bar{\alpha} = 30$ deg.

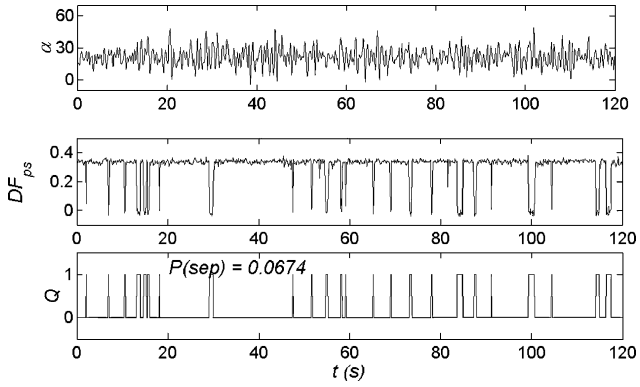

a) $\bar{\alpha} = 20$ deg

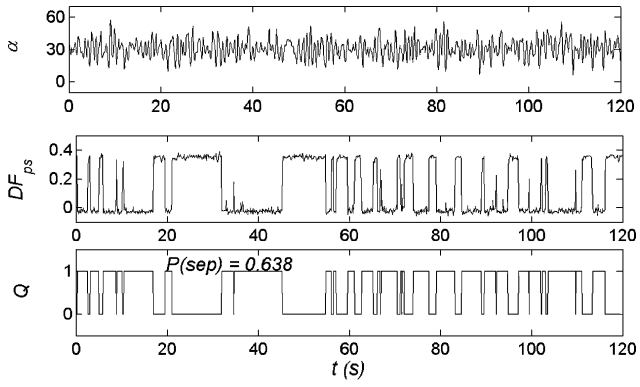

b) $\bar{\alpha} = 30$ deg

Fig. 9 Time traces following lip DF and separation for two mean wind directions, $Re = 3 \times 10^5$, $h/D_1 = 1$, $\overline{L_q}/D_1 = 3$, and $\phi = 0.62$.

Figure 9 shows time traces of the measured far-field wind angle and the lip DF at the datum operating condition: $\overline{L_q}/D_1 = 3$, $h/D_1 = 1$, $Re = 3 \times 10^5$, and $\phi = 0.62$. Figures 9 demonstrate how the lip response varies with the mean crosswind angle. At a mean angle of 20 deg, the nacelle intermittently separates, but quickly reattaches. As the mean angle is increased, the tendency to separate grows and the length of the separations increases. At a mean angle of 30 deg, the nacelle is separated for most of the time and it reattaches intermittently.

It is also instructive to consider the typical duration of the separations. Although the wind is gusting around quite rapidly, the frequency of separation and reattachment is much lower than that of the fluctuations in the far-field flow. The integral timescale for the flow, L_u/V_∞, is about 0.1 s, but at a mean flow angle of 30 deg, the separations last several seconds. This confirms the presence of intake hysteresis in unsteady flow. It appears that the intake is separated by a particular feature of the wind that latches the flow into a separated state. The flow remains separated until a further reattaching wind feature occurs, and the intake flow is attached again.

Figure 9 clearly demonstrates the bimodal behavior of the intake in unsteady crosswind. Similar switching between attached and separated states has been reported during engine tests.[11] A binary variable that describes the state of the intake flow can be defined with little ambiguity using the measured peak suction DF,

$$Q = \begin{cases} 0 \text{ (attached)} & \mathrm{DF_{ps}} \geq 0.15 \\ 1 \text{ (separated)} & \mathrm{DF_{ps}} < 0.15 \end{cases} \tag{7}$$

The variation of Q with time is in Fig. 9. When this parameter is used, a simple statistical measure can be defined that quantifies the proportion of the total time that the intake flow spends separated,

$$P(\text{sep}) = \frac{1}{T} \int_0^T Q(t)\, \mathrm{d}t \tag{8}$$

This statistical measure of the intake flowfield is a function of the nondimensional operating condition as shown in Eq. (2). Long-duration measurements of the intake lip pressure distribution were carried out at many operating conditions. These allowed the variation in $P(\text{sep})$ with the different experimental variables to be accurately determined.

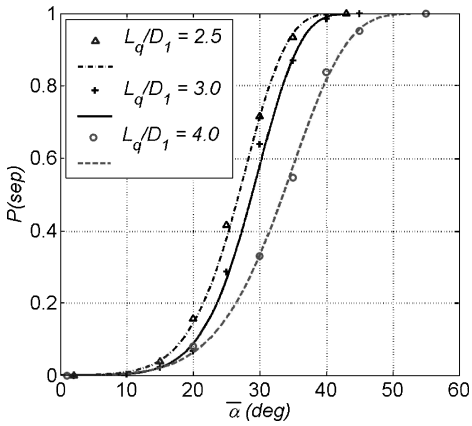

Fig. 10 Effect of stream-tube contraction ratio on probability of being separated, $Re = 3 \times 10^5$, $h/D_1 = 1$, and $\phi = 0.62$.

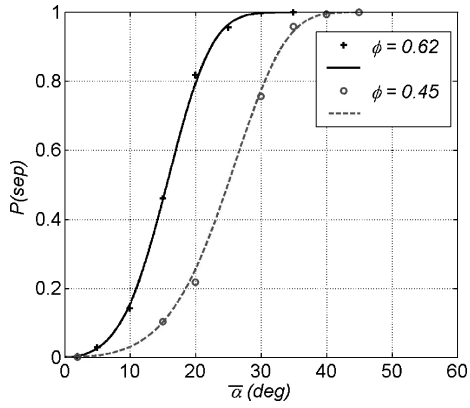

Fig. 11 Effect of fan flow coefficient on the probability of being separated, $Re = 2 \times 10^5$, $h/D_1 = 1$, and $\overline{L_q}/D_1 = 3$.

Figure 10 shows the effect of mean stream-tube contraction and crosswind angle on the probability of the intake being separated. Each of the points in the Fig. 10 is evaluated according to Eqs. (7) and (8), using over 6000 measurements of the nacelle surface pressure distribution. The probability varies from 0 to 1 over a range of flow angles, following a curve that has the typical shape of a cumulative probability distribution function.

The trends shown in Fig. 10 follow the observations made in the steady experiments. In steady flow, the rig operating with a high stream-tube contraction ratio was found to separate at a higher crosswind angle and reattach at a lower angle than when operating in a low stream-tube contraction ratio.[5] The lower gradient of the curve, $\mathrm{d}P(\text{sep})/\mathrm{d}\bar{\alpha}$, when $\overline{L_q}/D_1 = 4$, is analogous to the low rate of change of aerodynamic lip loading with flow angle in steady conditions. Also note that the entire transition range of angles measured in unsteady flow, from always attached to always separated, is below the steady-state crosswind angle at separation.

The influence of flow coefficient on the probability of the flow being separated is shown in Fig. 11. As the fan is moved toward stall, the likelihood of the intake being separated reduces. For example, at a crosswind angle of 20 deg, changing the operating point of the fan can change the proportion of time the flow spends separated from about 80 to 20%. This demonstrates that the fan has the same strong influence on the tendency for the intake to be separated in unsteady flow as it does in steady flow. Also note that the difference in gradient between the two curves suggests that the separation and reattachment of the intake are affected unequally.

In summary, the surface static pressure distributions measured in unsteady, attached flow are similar to those recorded at the equivalent

steady conditions. When the flow separates, the surface pressure distribution collapses and oscillates around a mean separated level. The attached and separated states of the flow are completely distinct, and the transitions between the two states show similarities with measurements made in steady flow.

There is evidence of separation hysteresis within the unsteady flow, and the effects of the experimental variables on the tendency for the intake to be separated follow the same trends measured in steady flow. Although we have not presented the data here, when separated, the mean level of distortion presented to the fan is also the same as that measured in steady flow.[12]

VI. Quasi-Steady Model of Unsteady Intake Separation

Because transitions between separated and attached flow take place rapidly relative to the time that the flow remains in that state, we will assume that transitions can be treated as instantaneous, discrete events. These events are not completely independent because each separation must be followed by a reattachment before another separation event can occur. However, if we consider the time intervals between consecutive separation and reattachment events, then the lengths of these intervals for when the flow is attached and when it is separated should be independent. These intervals are shown in Fig. 12.

When treated as independent events with stationary statistical properties, the probability of a separation occurring during a given time interval can be expected to obey Poisson-like statistics, and the time interval between such events should follow an exponential distribution with probability density functions:

$$p(t_{\text{att}}) = (1/\mu_{\text{att}}) \exp(-t_{\text{att}}/\mu_{\text{att}}) \tag{9}$$

$$p(t_{\text{sep}}) = (1/\mu_{\text{sep}}) \exp(-t_{\text{sep}}/\mu_{\text{sep}}) \tag{10}$$

that is, the probability that an attached intake will remain attached for a time between t and $t + \mathrm{d}t$ is given by $p(t)\,\mathrm{d}t$. The exponential distribution is characterized by a single parameter, μ_{att}, the average value of the duration of attached periods of intake flow.

These distributions are tested against the experimental measurements using probability plots, an example of which is presented in Fig. 13. Each point in Fig. 13 represents a measured time between a reattachment event and the following separation event. The

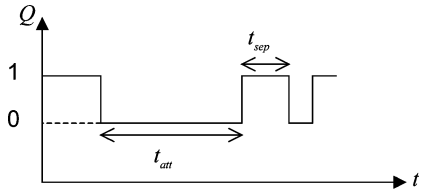

Fig. 12 Times between separation and reattachment events for the model rig.

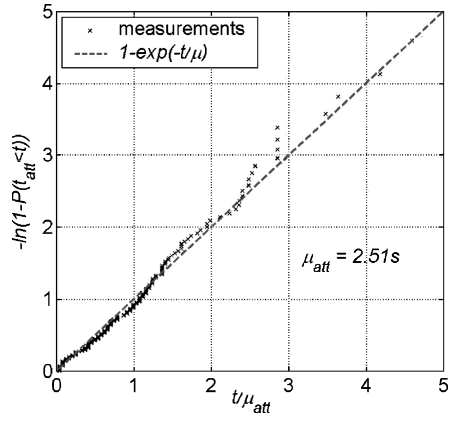

Fig. 13 Probability of time to separation after reattachment.

data have been ordered to produce a cumulative probability plot in which the y-axis ordinate has been chosen to give a straight line for the distribution given by Eq. (9) to aid comparison with the data. Figure 13 demonstrates that the intervals between the separation and reattachment events follow exponential statistics. Similar agreement is obtained at different operating conditions and for the times to reattachment t_{sep}. Note that, despite appearances, the line shown in Fig. 13 is not a best fit. It has been obtained by using the independently measured value of μ.

We will now consider the wind to be made up of a series of discrete, random gusts, each separated by an interval of time Δt. Physically this interval can be thought of as the minimum timescale to which the intake flowfield responds. The unsteady measurements suggest that the intake is most sensitive to gusts of a size comparable to the mean captured stream tube, and this observation will be used for a first estimate,

$$\Delta t \approx \overline{L_q}/V_\infty \tag{11}$$

The values chosen for the flow angle during the gusts are such that the probability distributions of the velocity fluctuations are the same as measured in natural wind. The statistics of velocity components, as given by the ESDU correlations, can be recast as a formula for a probability density function for flow angle variations,[12]

$$p(\beta) = \frac{V_\infty}{\sigma_v\left(\sigma_u^2\beta^2/\sigma_v^2 + 1\right)^{\frac{3}{2}}\sqrt{2\pi}} \exp\left\{\frac{V_\infty^2}{2\left(\sigma_u^2\beta^2/\sigma_v^2 + 1\right)\sigma_u^2}\right\}$$

$$\times \exp\left(\frac{-V_\infty^2}{2\sigma_u^2}\right) \qquad \beta = \tan(\alpha - \bar{\alpha}) = v/(V_\infty + u) \tag{12}$$

We will assume that the response of the intake flowfield is quasi steady so that the intake will separate and reattach when the gust value exceeds or reduces below the corresponding angle taken from the steady flow measurements in Ref. 5,

$$\alpha_s, \alpha_r = f\{Re_1, (h/D_1), (\overline{L_q}/D_1), \phi_f\} \tag{13}$$

A separating gust is, thus, defined as one that leads to a flow direction that exceeds the critical angle α_s. The probability of this occurring is given by

$$P(G_s) = P(\alpha > \alpha_s) = \int_{\alpha_s}^{\infty} p(\alpha)\,\mathrm{d}\alpha \tag{14}$$

Similarly, if a reattaching gust is one that produces a flow direction below the critical angle α_r,

$$P(G_r) = P(\alpha < \alpha_r) = \int_{-\infty}^{\alpha_r} p(\alpha)\,\mathrm{d}\alpha \tag{15}$$

These expressions can be found by simple (numerical) integration. A model of the wind is shown in Fig. 14.

The mean times to separation and reattachment as predicted by the model are

$$\mu_{\text{att}} = \Delta t/P(G_s) \qquad \mu_{\text{sep}} = \Delta t/P(G_r)$$

$$\text{provided} \quad \Delta t \ll \mu_{\text{sep}}, \mu_{\text{att}} \tag{16}$$

The latter condition is necessary for consistency between the assumptions that the wind can be considered as steady over time scale

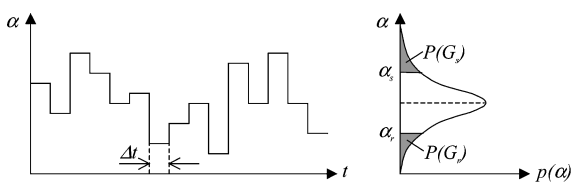

Fig. 14 Discrete gust model of natural wind.

Δt but unsteady over a time comparable with a typical length of a period of separation or attachment. The choice of Δt used does indeed satisfy this condition for the vast majority of measured events.

When the results in Eq. (16) are used, the following values are obtained for the predicted probability of separation and the predicted mean frequency of separation events:

$$P(\text{sep}) = \frac{\mu_{\text{sep}}}{\mu_{\text{sep}} + \mu_{\text{att}}} = \frac{P(G_s)}{P(G_s) + P(G_r)} \tag{17}$$

$$n_s = \frac{1}{\mu_{\text{att}} + \mu_{\text{sep}}} = \frac{1}{\Delta t} \frac{P(G_r)P(G_s)}{P(G_s) + P(G_r)} \tag{18}$$

When Eqs. (14) and (15) are solved, and the results are substituted into Eqs. (17) and (18), the results in Figs. 15 and 16 were obtained for the datum experimental condition. These results show good agreement with the measured values. Similar levels of agreement were obtained with all of the cases studied, and indeed, this agreement can be improved on when slightly more sophisticated models are used.[12] (Under steady conditions, α_r and α_s depend on stream-tube contraction ratio, the variation of this quantity in unsteady flow can be accommodated within the model.) Also shown for comparison in Figs. 15 and 16 are the values one would obtain using this model if hysteresis was ignored. That is, assuming the flow reattaches at the same wind angle as it separates.

To summarize, a model has been developed that is based on the intake flowfield responding quasi-steadily to fluctuations in the natural wind. The model uses a single timescale for the fluctuations in the wind and variations in wind speed and direction derived from Gaussian probability distributions. The criteria for separation and reattachment are derived from steady experimental results. It has been shown that this is sufficient to reproduce all of the trends observed in the statistics of the unsteady measurements.

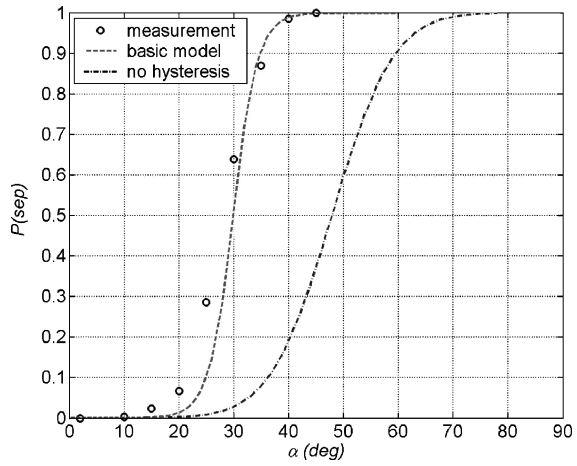

Fig. 15 Variation in probability of being separated for the model compared with test results, $Re = 3 \times 10^5$, $h/D_1 = 1$, $\phi = 0.62$, and $\overline{L_q}/D_1 = 3$.

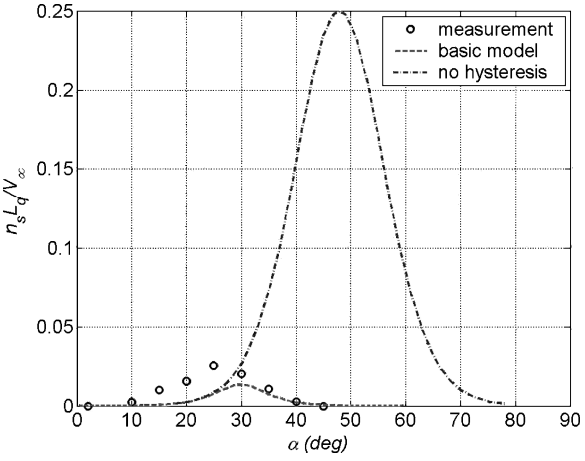

Fig. 16 Variation in frequency of separation events for basic model compared with test results, $Re = 3 \times 10^5$, $h/D_1 = 1$, $\phi = 0.62$, and $\overline{L_q}/D_1 = 3$.

VII. Implications for Full-Scale Engine Intakes

The experimental conditions used for the model rig experiments were, as far as possible, matched to the full-scale situation of an engine operating in atmospheric turbulence. Aspects of the model rig unsteady behaviour have also been observed in engine tests.[11,12] It is, therefore, expected that full-scale engine intakes, similar to the model rig, will respond quasi-steadily. This has the following technological implications.

1) The performance of an engine intake in steady crosswind can be related to its unsteady performance in natural wind. A method for doing this is demonstrated in the preceding section.

2) The most troublesome features of natural wind for an engine are the extreme quasi-steady gusts (where a quasi-steady gust is any variation in wind speed and direction that is large enough to engulf the captured stream tube). Thus, any test or computation aimed at demonstrating the tolerance of an engine to natural wind only needs to demonstrate the tolerance to the most extreme quasi-steady gusts.

3) For engine tests performed in a natural wind environment, the statistics of the quasi-steady gusts present in the local atmosphere should be determined. This will enable better interpretation of the measured intake performance.

4) Improved intake designs and better operational procedures could be developed by considering the statistics of the quasi-steady gusts that an engine will be exposed to during its lifetime. This possibility is explored in Ref. 13, in which it is concluded that intake design details and engine operational procedures can have a significant impact on the intake unsteady performance.

VIII. Conclusions

A new and novel experiment using a model fan and intake rig within simulated natural wind has been established. The setup effectively mimics aspects of the behavior of a full-scale engine in natural wind.

The unsteady measurements obtained show that as the model intake is approached all components of turbulence intensity are attenuated. Small-scale velocity fluctuations are effectively filtered out by the rapid acceleration of the flow into the intake, and it is the large-scale variations that are important. The inlet surface pressure field is most sensitive to fluctuations in the far field that are of a similar size to the captured stream tube.

A new statistical approach to analyzing intermittent intake separation has been presented. The results show that the model rig inlet exhibits significant hysteresis in the separation–reattachment cycle when operating within unsteady flow. Also, the effects of stream-tube contraction and fan operating point on the intake performance follow the same trends as those measured in steady flow. These new findings suggest that the response of the inlet flow-field can be described as quasi-steady, and a probabilistic model of intake behavior has been devised based on this hypothesis. This model successfully reproduces the statistics of the unsteady measurements, thus proving that the intake response is indeed quasi steady.

The response of a full-scale engine intake is also expected to be quasi-steady. This has implications for the testing, design, and operation of turbofan engines.

Acknowledgments

The authors are grateful for financial support for this work from Engineering and Physical Sciences Research Council and from Fan Systems, Rolls Royce, plc., and the encouragement of A. Rae throughout the research is greatly appreciated. The authors would like to acknowledge Fan Systems, Rolls–Royce, plc., for granting permission to C. A. Hall to carry out research at the Whittle Laboratory. They would also like to thank M. Whibley for the mechanical design and manufacture of the model rig. The use of the Osney wind

tunnel was with the kind permission and assistance of C. Wood, R. Belcher and M. Gamboa-Marrufo.

References

[1]Freeman, C., and Rowe, A. L., "Intake Engine Interactions of a Modern Large Turbofan Engine," *Proceedings of the International Gas Turbine and Aeroengine Congress*, American Scoiety of Mechanical Engineers, New York, 1999, Paper 99-GT-344.

[2]Bearman, P. W., and Morel, T., "The Effect of Free Stream Turbulence on the Flow Around Bluff Bodies," *Progress in Aerospace Science*, Vol. 20, No. 2–3, 1983, pp. 97–123.

[3]Britter, R. E., Hunt, J. C. R., and Mumford, J. C., "The Distortion of Turbulence by a Circular Cylinder," *Journal of Fluid Mechanics*, Vol. 92, 1979, pp. 269–301.

[4]Hunt, J. C. R., and Carruthers, D. J., "Rapid Distortion Theory and the 'Problems' of Turbulence," *Journal of Fluid Mechanics*, Vol. 212, 1990, pp. 497–532.

[5]Hall, C. A., and Hynes, T. P., "Measurements of Intake Separation Hysteresis in a Model Fan and Nacelle Rig," AIAA Paper 2002-3772, July 2002.

[6]Wood, C., "The Osney Laboratory Environmental Wind Tunnel," *Industrial Aerodynamics*, Vol. 4, No. 1, 1979, pp. 43–70.

[7]"Data Item 85020: Characteristics of Atmospheric Turbulence near the Ground. Part II: Single Point Data for Strong Winds," Engineering Science Data Unit International, Ltd., London, 1990.

[8]"Data Item 82026: Strong Winds in the Atmospheric Boundary Layer. Part I: Mean-Hourly Wind Speeds," Engineering Science Data Unit International, Ltd., London, 1982.

[9]Batchelor, G. K., *The Theory of Homogenous Turbulence*, Vol. 2. Cambridge Univ. Press, Cambridge, England, U.K., 1953, Chap. 4, pp. 68–75.

[10]Bearman, P. W., "Some Measurements of the Distortion of Turbulence Approaching a Two-Dimensional Bluff Body," *Journal of Fluid Mechanics*, Vol. 53, 1972, pp. 451–467.

[11]Sheaf, C., "Steady Crosswind Blower Measurements in a Strong Natural Wind," Rolls–Royce, plc., Derby, England, U.K., 2001.

[12]Hall, C. A., "Fan–Nacelle Interactions in Natural Wind," Ph.D. Dissertation, Engineering Dept., Univ. of Cambridge, Cambridge, England, U.K., Oct. 2002.

[13]Hall, C. A., and Humphreys, N. D., "Intake Performance During Rolling Take-Off in Natural Crosswind," AIAA Paper 2004-3403, July 2004.